Exponential time-scaling of estimation precision by reaching a quantum critical point

Louis Garbe [1], Obinna Abah [2,3], Simone Felicetti,[4] and Ricardo Puebla [3,5,6,*]

[1] *Vienna Center for Quantum Science and Technology, Atominstitut, TU Wien, 1040 Vienna, Austria*
[2] *School of Mathematics, Statistics and Physics, Newcastle University, Newcastle upon Tyne NE1 7RU, United Kingdom*
[3] *Centre for Theoretical Atomic, Molecular and Optical Physics, Queen's University Belfast, Belfast BT7 1NN, United Kingdom*
[4] *Istituto di Fotonica e Nanotecnologie, Consiglio Nazionale delle Ricerche (IFN-CNR), Via Cineto Romano 42, 00156 Rome, Italy*
[5] *Instituto de Física Fundamental, IFF-CSIC, Calle Serrano 113b, 28006 Madrid, Spain*
[6] *Departamento de Física, Universidad Carlos III de Madrid, Avenida de la Universidad 30, 28911 Leganés, Spain*

(Received 8 July 2022; accepted 4 October 2022; published 26 October 2022)

Quantum metrology refers to the use of quantum resources in parameter-estimation protocols, aiming at enhancing its precision. The quantum Fisher information is a key quantity in this context, setting the ultimate achievable precision with respect to available resources, such as the total time of the protocol. In this work, we report a scheme where the quantum Fisher information features an exponential scaling with the protocol duration. This is achieved by performing a periodic modulation of the coupling of a quantum critical system close to the its critical value. This modulation leads to an exponential growth of the excitation number in time. Relying on the precision bound derived by Garbe *et al.* [L. Garbe *et al.*, Quantum Sci. Technol. **7**, 035010 (2022)], we show that the quantum Fisher information inherits this exponential time scaling, which is corroborated by numerical simulations. Finally, the impact of dissipation and finite-size effects are analyzed, showing that the exponential time scaling is robust to dissipation, although its exponent decreases for larger values of the dissipation rate. Therefore, our work illustrates the novel metrological opportunities that quantum critical systems can offer.

DOI: 10.1103/PhysRevResearch.4.043061

I. INTRODUCTION

The existence of quantum fluctuations limits the precision that can be achieved in parameter-estimation protocols when using a limited number of physical resources. While the development of quantum mechanics has unveiled this fundamental limitation, it also provides us with the solution: By exploiting quantum resources, such as squeezing or entanglement, it is possible to overcome the fundamental limit of precision found for classical protocols [1–4]. Accordingly, quantum sensing is one of the most promising applications of current quantum technologies [5]. In the context of quantum metrology, in order to assess the performances of a parameter-estimation strategy, it is of utmost relevance to understand the scaling of the precision with respect to the amount of used resources, such as number of probes or total measurement time. At the theoretical level, the most common figure of merit to quantify the estimation precision is the quantum Fisher information (QFI), which sets the ultimate achievable precision according to the Cramér-Rao bound [3,6]. A paradigmatic example consists in the celebrated Heisenberg limit, valid under a series of very general assumptions [2], for which the QFI scales quadratically with the number of particles of the probe system and with the protocol duration time. This corresponds to a quadratic enhancement over the classical case, where the QFI scales linearly with those resources. It has also been shown that even super-Heisenberg scalings can be achieved when allowing for k-body interaction terms [7,8], in which case scalings N^{2k}, or potentially even exponential scaling in N, could be achieved (see, for example, [9]). Another possibility is to enable time-dependent Hamiltonian evolutions [10], which allows one to surpass the quadratic scaling in time.

In this context, systems undergoing critical phase transitions are ideal candidates for sensing applications, thanks to their high sensitivity to external perturbations. In particular, quantum phase transitions (QPTs) [11] represent a compelling resource [12–14] for quantum metrology due to highly nonclassical properties developed in proximity of the critical point. It has also been shown [15,16] that in spite of the critical slowing down, the framework of critical quantum metrology makes it possible to achieve the Heisenberg scaling, where the QFI grows quadratically in time and number of probes. Recent works [16–24] have shown that the framework of critical quantum metrology can be applied to a broad class of quantum optical models. Current solid-state and atomic technology allows for the implementation of these models in a controllable way, where their parameters can be tuned in real time. Intense research efforts [9,25–33] are now dedicated to identifying optimal control strategies that maximize the estimation precision while mitigating potential errors.

In this article, we present the design of a quantum sensing protocol that goes beyond the typical power-law scaling of the

*rpueblaantunes@gmail.com

QFI, achieving an exponential scaling with respect to protocol duration time. The protocol is based on a quantum-control strategy that exploits the critical nature of a QPT by cyclically bringing the probe system in proximity of the critical point. This modulation is intrinsically nonadiabatic, as at the critical point the energy gap closes. Information about the parameter describing the Hamiltonian is continuously encoded in the dynamics. By measuring the state at the end of the evolution, we can then reconstruct these parameters. This scheme is therefore an active interferometric metrological protocol where the number of probes N changes in time, and indeed increases exponentially with the number of cycles performed. Using both detailed numerical simulations and the analytical bound recently introduced in Ref. [25], we show that this exponential time growth of N is carried over to the estimation precision. Furthermore, in order to characterize the performances of the proposed protocols for practical applications, we analyze the effect of dissipative processes and of finite-size corrections. We find the protocol to be resilient to thermal and dissipative effects, and the exponential scaling is preserved when the decay rate is comparable to or smaller than the single-cycle time. The rate in the exponential scaling, however, gradually degrades with decoherence. As we explain, this corresponds to a departure from a Heisenberg (quadratic in N) to a standard-quantum (linear in N) regime. Finite-size corrections impose a saturation on the number of excitations, and so they constrain the maximum number of cycles allowed. The proposed protocol can be advantageous when the estimation time is the most relevant resource and when using quantum platforms where ground-state cooling is challenging.

II. CRITICAL FULLY CONNECTED MODEL

Among the different families of quantum critical systems, we focus on fully connected models such as the quantum Rabi, the Lipkin-Meshkov-Glick [34], and the Dicke [35] models. In the thermodynamic limit, these systems feature a QPT that divides the phase diagram in a normal and a symmetry-broken phase [36–44]. In the Dicke and Lipkin-Meshkov-Glick models, the thermodynamic limit refers to the standard notion of infinitely many components. In the quantum Rabi model, and related finite-component critical systems [45–51], it rather refers to a certain ratio of the system parameters. For instance, in the quantum Rabi model, a QPT emerges when the qubit frequency becomes much larger than the field frequency. The frequency ratio acts as an effective system size, and finite-size critical exponents can also be defined in this case. These models constitute a suitable testbed for the exploration of different aspects of quantum critical phenomena [45,46,48,49,52–66]. These fully connected systems admit a simple description in terms of an effective bosonic mode. For instance, let us consider the simple Rabi model describing the interaction between a qubit and a bosonic mode. Under a suitable Schrieffer-Wolff transformation, we can decouple the qubit and obtain an effective description in terms of the bosonic field [38,64],

$$H = \omega a^\dagger a - \frac{\lambda^2}{\Omega}(a + a^\dagger)^2, \tag{1}$$

where $[a, a^\dagger] = 1$, λ is the dimensionful coupling strength, and ω and Ω are the frequency of the field and qubit, respectively. The phase transition occurs at $\lambda = \lambda_c = \frac{\sqrt{\omega\Omega}}{2}$. We can then rewrite this model in the following form:

$$H = \omega\left[a^\dagger a - \frac{g^2}{4}(a + a^\dagger)^2\right]. \tag{2}$$

This structure makes apparent that the critical dynamics is entirely described by two parameters: a global energy scale ω and a renormalized, dimensionless coupling strength g which modulates the potential of the bosonic field. The transition then takes place for $g = g_c = 1$. This derivation can be carried out with other fully connected systems, such as the Lipkin-Meshkov-Glick (LMG) model (see Ref. [25] for details), leading to the same effective Hamiltonian.

The distance to the transition point, $g - g_c$, is the most important parameter in this effective description. In particular, observables will obey critical scalings with this distance; for instance, the energy gap vanishes at the QPT as $\Delta(g) \propto |g - g_c|^{1/2}$. The associated critical exponents in this case are of a mean-field type, $z\nu = 1/2$ [11]. It is worth stressing that the critical traits in these systems have been experimentally observed [67–72].

It is important to notice that, in general, ω and g will not be independent. For instance, in both the Rabi and LMG model, we have $g \propto 1/\sqrt{\omega}$. Hence, in all of these models, changing the frequency ω will both rescale the model frequency *and* the distance to the critical point. In the present and our previous study [25], we exploit this circumstance to devise a sensing protocol critically dependent on the value of ω.

Finally, let us comment on possible experimental implementations of critical fully connected models, which could be realized using current technology. Notice that we are making two strong assumptions on the coupling parameter g, as an implementation of the proposed protocols requires that (i) g can be fast-modulated in real time and (ii) g can be made large enough to approach the critical point. These requirements can both be achieved with effective implementations, where a coupling is induced by an external parametric pump. A broad variety of methods to induce effective couplings have been experimentally demonstrated, making it possible to observe critical phase transitions and access extreme coupling regimes in neutral atoms [68,73,74], trapped ions [72,75–77], circuit QED [78–80], optomechanical devices [81,82], and nuclear magnetic resonance [83], as a nonexhaustive list.

III. QUANTUM FISHER INFORMATION

The ultimate precision for the estimation of a parameter o is given by the QFI [3], denoted as I_o, such that the variance for the estimated parameter o is bounded as $(\delta o)^2 \geqslant I_x^{-1}$ for a single measurement, which is known as the quantum Cramér-Rao bound. This result is obtained optimizing over all possible positive operator-valued measurements and classical data processing. Thus, the scaling of I_o with respect to the experimental resources, such as the duration of the metrological protocol, is of key importance. Let us denote ρ_o as the system state in which the unknown value of o has been encoded. The QFI is related to the Bures distance between

two infinitesimally closed states, ρ_o and $\rho_{o+\epsilon}$, which can be written as $d^2_{\mathrm{B},o} = 2(1 - \mathrm{Tr}[\sqrt{\sqrt{\rho_o}\rho_{o+\epsilon}\sqrt{\rho_o}}])$, so that [84]

$$I_o = 4\left(\frac{\partial d_{\mathrm{B},o}}{\partial \epsilon}\bigg|_{\epsilon=0}\right)^2. \tag{3}$$

The signal-to-noise ratio can then be written as $Q_o = o^2 I_o$.

Since the Hamiltonian (2) is quadratic in a and $a^\dagger$, any initial Gaussian state evolving under (2) remains Gaussian [85]. Recall that a Gaussian state ρ is that whose Wigner function is Gaussian, and thus ρ can be fully determined in terms of its first and second moments in the two-dimensional phase space, $\mathbf{X}^\top = (X_1, X_2) = (x, p)$ [85], where here we employ the convention $x = a + a^\dagger$ and $p = i(a^\dagger - a)$. The first moments of the state are simply $\langle \mathbf{X}^\top \rangle = (\mathrm{Tr}[\rho\ x], \mathrm{Tr}[\rho\ p])$. The second moments are given by the covariance matrix $\mathbf{R}$, which is real and symmetric, and its matrix elements read as

$$R_{i,j} = \tfrac{1}{2}\langle X_i X_j + X_j X_i\rangle - \langle X_i\rangle\langle X_j\rangle. \tag{4}$$

As shown in Ref. [84], the QFI adopts the following form for Gaussian states:

$$I_o = \frac{1}{2}\frac{\mathrm{Tr}[(\mathbf{R}^{-1}\partial_o \mathbf{R})^2]}{1+P^2} + 2\frac{(\partial_o P)^2}{1-P^4} + L_o, \tag{5}$$

with $L_o = \boldsymbol{\Delta}\mathbf{X}_o'^{\top}\mathbf{R}^{-1}\boldsymbol{\Delta}\mathbf{X}_o'$ and $\boldsymbol{\Delta}\mathbf{X}_o' = \partial\langle \mathbf{X}_{o+\epsilon} - \mathbf{X}_o\rangle/\partial\epsilon|_{\epsilon=0}$, and $P = \det[\mathbf{R}]^{-1/2}$ denotes the purity of the Gaussian state ρ. Throughout the article, we will consider Gaussian states with $\langle x\rangle = \langle p\rangle = 0$, and therefore $L_o = 0$ in Eq. (5). In this manner, the QFI and the corresponding signal-to-noise ratio Q_o can be computed from the covariance matrix $\mathbf{R}$. In the following, we will focus on the estimation of the bosonic frequency ω, although similar results can be found for the estimation of g in Eq. (2).

IV. NONADIABATIC CYCLES: EXPONENTIAL SCALING

The Hamiltonian in Eq. (2) displays a QPT at the critical point $g_c = 1$, which is accompanied by a vanishing energy gap, among other features. As a consequence, by tuning $g(t)$ towards the QPT in a finite time, the system will unavoidably depart from adiabaticity [86,87]. Such nonadiabaticity translates in the formation of quantum excitations in the system, which can be harnessed and beneficial in different contexts [88]. In the following, we show that the nonadiabaticity caused by the QPT can be exploited to lead in an exponential scaling of the QFI with respect to the protocol duration.

In particular, we choose a protocol $g(t)$ that completes a cycle in a time $2\tau \gtrsim 1/\omega$ as (cf. Fig. 1)

$$g(t) = \begin{cases} g_\tau \frac{t}{\tau} & \text{for } 0 \leqslant t \leqslant \tau \\ g_\tau\left(2 - \frac{t}{\tau}\right) & \text{for } \tau \leqslant t \leqslant 2\tau, \end{cases} \tag{6}$$

so that $g(0) = 0$ and $g(\tau) = g_\tau$. The state at any time t follows from $\dot\rho = -i[H(t), \rho(t)]$, with the initial and final state upon the completion of the cycle given by $\rho(0)$ and $\rho(2\tau)$, respectively. Note that the condition $2\tau \gtrsim 1/\omega$ rules out fast cyclic transformation ($\omega\tau \to 0$) for which the initial state remains trivially unchanged. If we perform a cycle away from the critical point, i.e., for $g_\tau < g_c = 1$, and for sufficiently slow cycles, $\tau \gg 1/\Delta(g_\tau)$, the protocol is able to meet the adiabatic condition. Hence, by virtue of the adiabatic theorem, the state upon the cyclic transformation is simply $\rho(2\tau) = \rho(0)$. By contrast, if we bring the system all the way to the critical point, i.e., if $g_\tau = g_c = 1$, the adiabatic condition will break down at some point since $\Delta(g_c) = 0$. Thus, $\rho(2\tau) \neq \rho(0)$ regardless of how slow the cycle is performed, as studied in Ref. [87]. Indeed, the transformation (6) reaching the critical point produces squeezing, that is, $\rho(2\tau) = \mathcal{S}(s)\rho(0)\mathcal{S}^\dagger(s)$ with $\mathcal{S}(s) = \exp[(s(a^\dagger)^2 - s^* a^2)/2]$ and $s = |s|e^{i\theta}$, with $|s|$ and θ the squeezing parameter and its angle, respectively. In this manner, the state is squeezed along $\mathbf{x}_s^\top = [\cos(\theta/2), \sin(\theta/2)]$ in the phase space. To a good degree of approximation (cf. Appendix A), the acquired squeezing after completing the protocol $g(t)$ with duration 2τ (and $\tau \gtrsim 1/\omega$) is given by [87,88]

$$|s| = \frac{\ln(3)}{2} \approx 0.55, \tag{7}$$

while the angle θ depends on τ (see Fig. 1). Note that this is caused solely by the presence of the QPT.

Although setting $g_\tau = 1$ allows one to automatically break adiabaticity, the resulting squeezing is robust against small deviations from $g_\tau = 1$, i.e., for cycles with $|g_\tau - g_c| \ll 1$, Eq. (7) still holds for $1/\omega \lesssim \tau \lesssim 1/\Delta(g_\tau)$ (cf. Appendix A).

This cyclic transformation can be carried out m times by a concatenation of the protocol $g(t)$ in (6), that is, $g(t + 2m\tau) = g(t)$ with $t \in [0, 2\tau]$ and $m = 1, 2, \ldots$, in a total time $T = 2m\tau$. By doing so, the produced squeezing can be amplified to yield $|s_m| = m|s| = m\ln(3)/2$, where $|s_m|$

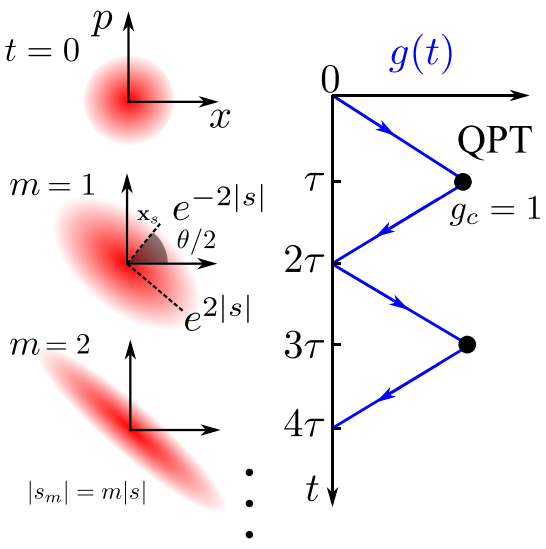

FIG. 1. Schematic illustration of the protocol. At $t = 0$, the state is assumed to be in a vacuum or thermal state, which is brought to the critical point $g_\tau = g_c = 1$ in a time τ by tuning $g(t)$. The cycle is completed at time 2τ such that $g(2\tau) = g(0) = 0$. After one cycle $m = 1$, the state becomes squeezed, with a squeezing parameter and angle $|s|$ and θ, respectively, so that the state is squeezed along the direction $\mathbf{x}_s^\top = [\cos(\theta/2), \sin(\theta/2)]$ in the phase space $\mathbf{X}^\top = (x, p)$, reducing the variance by a factor $e^{-2|s|}$. Performing another cycle, $m = 2$, the state can be further squeezed such that $|s_m| = m|s|$, where $m = 1, 2, \ldots$, under suitable parameters. This squeezing amplification leads to an exponential precision for the estimation of the system parameters (see main text for further details).

denotes the squeezing produced on the initial state $\rho(0)$ after the mth cycles, i.e., $\rho(2m\tau) = \mathcal{S}(s_m)\rho(0)\mathcal{S}(s_m)$ with $s_m = |s_m|e^{i\theta_m}$ (cf. Fig. 1). Such amplification requires a phase-matching condition for subsequent cycles, i.e., $\theta_{m+1} = \theta_m$. However, if $\theta_{m+1} = \theta_m + \pi$ (modulo 2π), the $(m+1)$th cycle compensates the squeezing generated in the previous cycle, and thus we expect $|s_{2m+1}| \approx |s| = \ln(3)/2$ and $|s_{2m}| \approx 0$, so that $N_{2m+1} \approx N_{m=1} = 1/3$ while $N_{2m} \approx 0$.

It is worth mentioning that other schemes can also achieve a linear amplification of squeezing, such as the one reported in Ref. [32] based on a suitable periodic modulation of the oscillator frequency [89], which differs from Eq. (6).

A. Bound to the quantum Fisher information

As aforementioned, Eq. (5) allows us to exactly compute the QFI. However, before presenting the numerical results in the next section, here we show that the main features of the QFI behavior can be predicted analytically. For that, we rely on a recently derived bound to the QFI, which is valid for active interferometric protocols and Gaussian states. This bound is denoted as I_ω^{B} such that $I_\omega \leqslant I_\omega^{\mathrm{B}}$, and in our case is given by (see Ref. [25] for the details of the derivation)

$$I_\omega^{\mathrm{B}} = 8(\chi^2 + \phi^2)\left\{\int_0^T dt[2N(t)+1]\right\}^2, \tag{8}$$

where $N(t)$ denotes the number of bosons at time t, while χ and ϕ are the eigenvalues of the matrix $\partial_\omega H(t)$ in the phase space $\mathbf{X}$, which here take a time-independent value $\chi = \phi = 1/2$ [25]. If the number of probes $N(t)$ is time independent, Eq. (8) returns the Heisenberg scaling N^2T^2. By contrast, if $N(t)$ is time dependent, which is the case here, we can achieve more exotic scalings in T. For simplicity, let us consider an initial vacuum state $\rho(0) = |0\rangle\langle 0|$, although we remark that the results are robust against finite-temperature initial states (see Appendix B). From Eq. (7) and since $N = \mathrm{Tr}[\mathcal{S}(s)\rho(0)\mathcal{S}^\dagger(s)a^\dagger a] = \sinh^2(|s|)$, we expect the number of bosons, $N_m = \mathrm{Tr}[\rho(2m\tau)a^\dagger a]$, after m cycles, assuming a phase-matching condition, to obey

$$N_m = \sinh^2\left[\frac{m}{2}\ln(3)\right], \tag{9}$$

which grows exponentially with m, $N_m \sim 3^m/4$ for $m \gg 1$. Hence, we can already anticipate that I_ω^{B} will show a similar exponential scaling. Indeed, by approximating $N(t)$ during $t \in [2(m-1)\tau, 2m\tau]$ by N_m so that $\int_{(2m-1)\tau}^{2m\tau} dt\,[2N(t)+1] \approx 2\tau(2N_m+1)$, we find

$$\begin{aligned} I_\omega^{\mathrm{B}} &\leqslant 16\tau^2(2N_m+1)^2 \\ &\approx 64\tau^2\sinh^4[m\ln(3)/2], \end{aligned} \tag{10}$$

where, in the last step, we have assumed $N_m \gg 1$. In this manner, for $m \gg 1$, we find

$$I_\omega^{\mathrm{B}} \approx 4\tau^2 3^{2m} = 4\tau^2 3^{T/\tau}, \tag{11}$$

where $T = 2m\tau$ is the total time of the protocol after m cycles. That is, the bound to the QFI scales exponentially with T. This is the central result of the article. Note that I_ω^{B} does not surpass the Heisenberg limit since it still corresponds to $T^2N_m^2$. The improvement in the time-scaling comes from the fact that the number of probes, N_m, increases in time. It is worth mentioning that if we have a standard-quantum-limited scaling, $I_\omega^{\mathrm{SQL}} \propto N_m$ instead of N_m^2 as in Eq. (10), we would obtain $I_\omega^{\mathrm{SQL}} \sim 3^m$, so both scale exponentially with the number of cycles. However, $I_\omega^{\mathrm{B}} \sim 3^m I_\omega^{\mathrm{SQL}}$, meaning that the Heisenberg behavior still provides an exponential advantage with respect to the standard-quantum behavior.

In the remainder of the article, we will employ numerical simulations to corroborate the validity of Eq. (11) (cf. Sec. IV B), while in Sec. V, we investigate the noise robustness of such exponential scaling and how the QFI tends to I_ω^{SQL} as decoherence becomes prominent, as well as to analyze the potential impact of finite-size effects.

B. Noiseless dynamics in the thermodynamic limit

The dynamics in the thermodynamic limit can be computed exploiting the quadratic nature of the Hamiltonian (2). Assuming that the initial state is such that $\langle x\rangle = \langle p\rangle = 0$ and that it undergoes a noiseless evolution under the protocol $g(t)$, the state at time t is completely characterized by the following time-dependent Lyapunov equation of motion for the covariance matrix (see Appendix C):

$$\dot{\mathbf{R}}(t) = \mathbf{W}(t)\mathbf{R}(t) + \mathbf{R}(t)\mathbf{W}^\dagger(t), \tag{12}$$

with

$$\mathbf{W}(t) = \begin{bmatrix} 0 & \omega[1-g^2(t)] \\ -\omega & 0 \end{bmatrix}, \tag{13}$$

while $\langle x\rangle = \langle p\rangle = 0\ \forall t$. The number of bosons at time t is then given by $N(t) = \frac{1}{4}\{\mathrm{Tr}[\mathbf{R}(t)] - 2\}$, while the QFI can be computed exactly using Eq. (5) and compared with the bound prediction (11). In order to test the prediction of the exponential scaling for I_ω, we consider $\rho(0) = |0\rangle\langle 0|$ so that $\mathbf{R}(0) = \mathbb{I}$. Numerically solving Eq. (12) under the protocol $g(t)$ given in Eq. (6), we can compute $N_m = N(2m\tau)$ and the corresponding signal-to-noise ratio $Q_\omega = \omega^2 I_\omega$. The phase-matching condition is achieved here when $\omega\tau = 2n$ with $n = 1, 2, \ldots$, so that $\theta_m = \pm\pi/2\ \forall m$, while for $\omega\tau = 2n+1$, the $(m+1)$th cycle counteracts the generated squeezing in the previous one (cf. Appendix C). Thus, for the phase-matching condition, the state is squeezed in the direction $\mathbf{x}_s^\top = (1, \pm 1)/\sqrt{2}$ in the phase space. The number of bosons after m cycles is plotted in Fig. 2(a) for $\omega\tau = 8$ (phase-matching condition), $\omega\tau = 8.2$, and $\omega\tau = 9$. The results clearly show the exponential growth of N_m, which is well captured by Eq. (9), for $\omega\tau = 8$. Finally, the signal-to-noise ratio Q_ω is plotted in Fig. 2(b), together with the bound and its approximated value given in Eq. (8) and (11), respectively. The numerical results show that the QFI shows an exponential scaling with the protocol duration T, $Q_\omega \propto 3^{T/\tau}$, as predicted by Eq. (11). The exponential scaling still holds, although the prefactor is reduced, in situations when $\omega\tau \sim 2n$ but $\omega\tau \neq 2n$, as exemplified by $\omega\tau = 8.2$. On the contrary, for $\omega\tau = 2n+1$, the number of bosons is bounded by $1/3$, which leads to the standard $Q_\omega \propto T^2$ scaling. We stress again that although the previous results have been computed considering $\rho(0) = |0\rangle\langle 0|$, i.e., a zero-temperature initial state, initial thermal states with an arbitrary temperature also lead to an exponential advantage (cf. Appendix B).

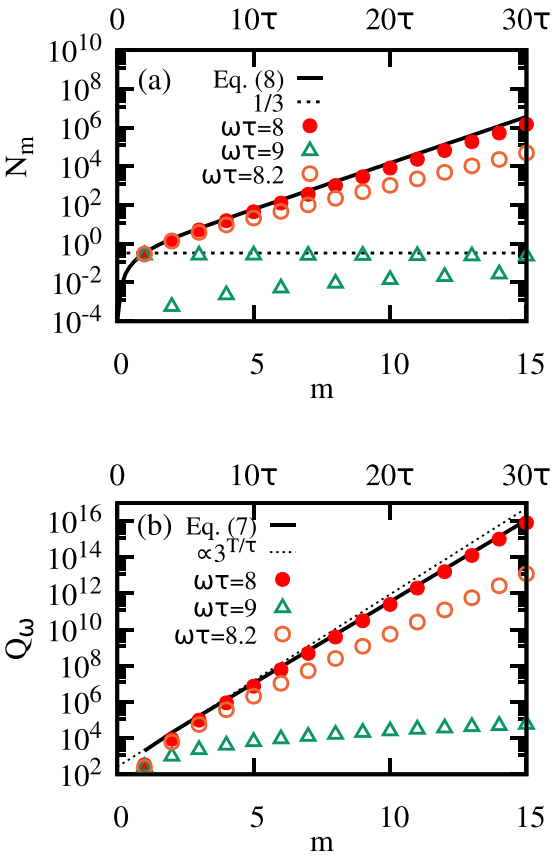

FIG. 2. Noiseless dynamics in the thermodynamic limit for an initial vacuum state. (a) Number of bosons after m cycles, N_m, for $\omega\tau = 8$ (solid red circles), $\omega\tau = 9$ (open green triangles), and $\omega\tau = 8.2$ (open orange circles). The phase-matching condition is achieved for $\omega\tau = 8$, which leads to an exponential growth of N_m, while for $\omega\tau = 9$, it follows that $N_{2m+1} \approx 1/3$ (dotted black line) (see main text). The results for $\omega\tau = 8$ follow the trend predicted in Eq. (9) (solid black line), which is closely followed by small deviations from the phase-matching condition, as illustrated for $\omega\tau = 8.2$. (b) Computed signal-to-noise ratio $\mathcal{Q}_\omega = \omega^2 I_\omega$ together with the bound computed numerically using Eq. (8) (solid black line) as well as its approximated expression (dotted black line), given in Eq. (11), i.e., $I_\omega^{\mathrm{B}} \approx 4\tau^2 3^{T/\tau}$. The exponential scaling is robust against deviations from the phase-matching condition. For $\omega\tau = 9$, there is no exponential scaling, but rather $\mathcal{Q}_\omega \propto (2m\tau)^2 = T^2$, which is also well captured by the bound (not explicitly shown).

Let us conclude this section by commenting on the attainability of the QFI. The QFI bound gives the maximum precision achievable when optimizing over all possible observables. This then begs the question, which observables allow one to reach or approach this maximum? In a previous work of ours [25], we studied a similar protocol, in which the coupling of a fully connected system was modulated in time to generate time-dependent squeezing, leading to a QFI that scales polynomially in time. We also studied the achievability of the QFI bound and found that it could, in general, be saturated using standard homodyne measurement or photon counting. Although the time-scalings that we obtain in the present work are very different, the resulting states are similar (essentially time-dependent squeezed thermal states) and we expect that the QFI here should be reachable as well using these standard methods.

V. NOISE ROBUSTNESS AND FINITE-SIZE EFFECTS

Let us now analyze the robustness of the exponential scaling in the QFI with respect to decoherence. For that, we model the interaction of the system with an environment at an inverse temperature β such that $N_{\mathrm{th}} = (e^{\beta\omega} - 1)^{-1}$ through the standard Lindblad master equation [90]

$$\dot{\rho}(t) = -i[H(t), \rho(t)] + \mathcal{D}[\rho(t)], \tag{14}$$

where the dissipator reads as

$$\mathcal{D}[\rho] = \kappa \frac{(N_{\mathrm{th}} + 1)}{2}(2a\rho a^\dagger - \{a^\dagger a, \rho\}) \tag{15}$$

$$+\kappa \frac{N_{\mathrm{th}}}{2}(2a^\dagger \rho a - \{aa^\dagger, \rho\}), \tag{16}$$

and the parameter κ accounts for the system-environment interaction strength. As the master equation is still quadratic in a and $a^\dagger$, the time-dependent Lyapunov equation for the covariance matrix modifies to

$$\dot{\mathbf{R}}(t) = \tilde{\mathbf{W}}(t)\mathbf{R}(t) + \mathbf{R}(t)\tilde{\mathbf{W}}^\dagger(t) + \mathbf{F}, \tag{17}$$

where now $\mathbf{F} = \kappa(2N_{\mathrm{th}} + 1)\mathbb{I}$ and $\tilde{\mathbf{W}} = \mathbf{W} - \kappa/2\mathbb{I}$. As before, we compute the $\mathcal{Q}_\omega$ from Eq. (5) solving Eq. (17). The results are gathered in Fig. 3(a) for $N_{\mathrm{th}} = 2$, which shows that the exponential scaling is robust against decoherence provided $2\tau\kappa \ll 1$. There we show $\mathcal{Q}_\omega$ for different values of κ starting from $\rho(0) = |0\rangle\langle 0|$. For $2\tau\kappa \ll 1$, the dissipation still permits an exponential scaling $\mathcal{Q}_\omega \propto 3^{\alpha m} = 3^{\alpha T/(2\tau)}$, but with smaller prefactor, $0 < \alpha \leqslant 2$, which is reduced as κ increases. On the contrary, for $2\tau\kappa \gg 1$, the state relaxes to the thermal equilibrium before the cycle is completed and thus $\mathcal{Q}_\omega$ does not increase with the protocol duration. For $2\tau\kappa \approx 1$, both mechanisms are balanced and $\mathcal{Q}_\omega \propto T^2$ is still possible. Since $\mathcal{Q}_\omega \propto 4\tau^2 3^{2m}$, for a fixed number of cycles m, the QFI is maximal when $2\tau\kappa = 1$ provided $\omega\tau$ ensures the phase-matching condition, while for fixed total evolution time T, it is more beneficial to perform the largest allowed number of cycles $m = T/(2\tau)$, and hence to take the shortest possible τ, with the constraints $2\tau \gtrsim 1/\omega$ and $2\tau\kappa \ll 1$. After m cycles, the system finds itself in a squeezed thermal state, so that the variance along the squeezing axis reads as $(\Delta\mathbf{x}_s)^2 = (2n_\kappa + 1)e^{-2|s_m|}$, while $(\Delta\mathbf{p}_s)^2 = (2n_\kappa + 1)e^{2|s_m|}$ is enlarged, where n_κ is the number of thermal bosons acquired by the state due to the interaction with the environment which decreases its purity, that is, $\mathrm{Tr}[\rho(2\tau m)^2] = (2n_\kappa + 1)^{-1}$. For $\kappa = 0$, the state remains pure and $n_\kappa = 0$. Moreover, the total number of bosons after m cycles is $N(2\tau m) = (2n_\kappa + 1)\sinh^2|s_m| + n_\kappa$. Although $|s_m|$ increases with m for $2\tau\kappa \lesssim 1$, so does the number of thermal bosons. This leads to a saturation in the variance $(\Delta\mathbf{x}_s)^2$, while $(\Delta\mathbf{p}_s)^2$ keeps increasing with m, which still allows $\mathcal{Q}_\omega$ to grow. This is shown in Fig. 3(b). For $2\tau\kappa > 1$, both quadratures saturate and, therefore, also $\mathcal{Q}_\omega$. In addition, we also show the behavior of the prefactor α as a function $2\tau\kappa$, which is illustrated in Fig. 3(c). There we show the fitted α such that $\mathcal{Q}_\omega \propto 3^{\alpha m}$. For a noiseless evolution, $\alpha \approx 2$ [see Fig. 2(b) and Appendix A for a comment regarding the expected deviation with respect to $\alpha = 2$],

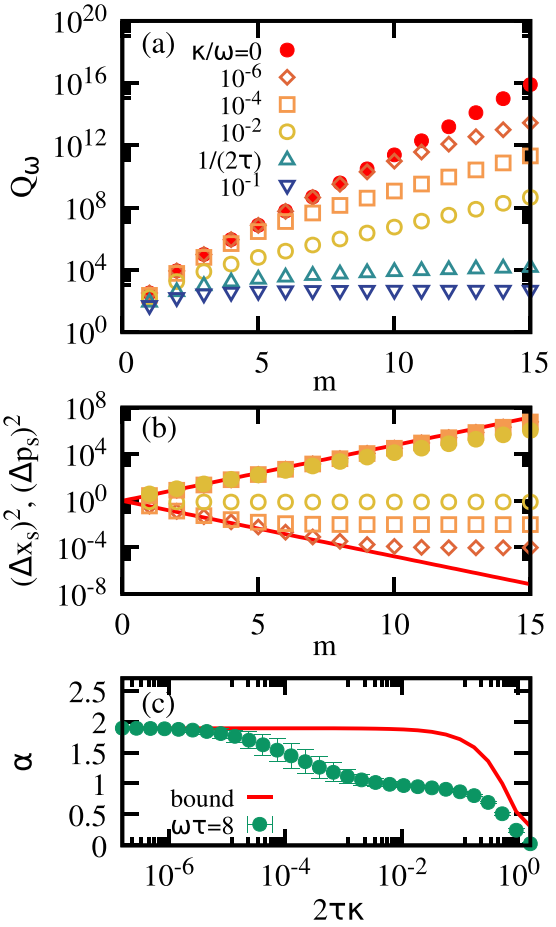

FIG. 3. Robustness of the exponential scaling in Q_ω vs decoherence effects. The results have been obtained for $\rho(0) = |0\rangle\langle 0|$, $g_\tau = g_c = 1$, and $\omega\tau = 8$ as in Fig. 2, although equivalent results can be found for different $\omega\tau \gtrsim 1$. (a) Q_ω for increasing number of cycles m, (b) variance along the squeezing axes, and (c) prefactor α such that $Q_\omega \propto 3^{\alpha m}$, obtained as a best fit in the interval $m \in [5, 10]$, as a function of $2\tau\kappa$. In (b) the solid red line corresponds to $3^{\pm m}$, as expected theoretically for $\kappa = 0$. Open [full] points correspond to $(\Delta \mathbf{x}_s)^2$ [$(\Delta \mathbf{p}_s)^2$] with the same format as in (a). In (b), the solid red line corresponds to α obtained from a fit to the bound in Eq. (8). The exponential advantage holds even for nonzero dissipation interaction strength κ, although the prefactor α in the scaling decreases. For $2\tau\kappa = 1$ [open yellow triangle in (a) and (b)], the scaling shifts to the standard quadratic scaling $Q_\omega \propto T^2$, while for $2\tau\kappa > 1$, the signal-to-noise ratio Q_ω saturates and $\alpha = 0$. Note that α shows a plateau at $\alpha = 1$, which can be interpreted as a standard-quantum limit behavior (see main text).

while as κ increases, $\alpha \to 0$. Yet, there is a wide range of values for κ in which the exponential scaling holds. Similar results can be found for other $\omega\tau$ fulfilling (or close to) a phase-matching condition. For comparison, we also compute α using the bound in Eq. (8). As shown in Fig. 3(b), although the bound still captures the exponential scaling for $2\tau\kappa \lesssim 1$, it becomes loose and overestimates the exponent α. As we show in Fig. 3(c), the exponent α gradually decreases with increasing decay rate κ, and shows a plateau at the value 1. Finally, when κ is further increased, α starts decaying again and finally reaches 0, at which point the precision becomes independent of the protocol duration. It is worth mentioning that the transition from $\alpha = 2$ to 1 can be understood as a departure from the Heisenberg to the standard-quantum limit. Indeed, we can reexpress Q_ω in terms of both the maximum number of bosons and the protocol duration time. Then, $\alpha = 2$ corresponds to $Q_\omega \sim N_m^2 T^2$ (Heisenberg limit), while $\alpha = 1$ to $Q_\omega \sim N_m T$, which is the scaling of the standard-quantum limit. This expression is useful if we are in a situation in which both the protocol duration and the number of photons are limited. By contrast, if the only relevant resource is the time, we can express again $N_m \sim 3^m = 3^{T/\tau}$. As aforementioned, both $\alpha = 1$ and $\alpha = 2$ lead to an exponential scaling of the QFI with T, yet $\alpha > 1$ corresponds to an exponential advantage with respect to the standard-quantum limit.

Finally, we turn our attention to finite-size effects. As commented in Sec. II, the Hamiltonian H in Eq. (2) is valid in the normal phase and in the thermodynamic limit. Yet, any realistic exploration of a critical system is unavoidably accompanied by finite-size corrections. Let us denote by η the system size, which in the Lipkin-Meshkov-Glick and quantum Rabi models refers to the number of spins and a ratio between spin and bosonic frequencies, respectively. Indeed, for $\eta < \infty$, the leading-order correction to Eq. (2) leads to a Hamiltonian of the form $H_\eta = H + \frac{f(g)}{\eta}(a + a^\dagger)^4$, where $f(g)$ is a function of g [25,64]. In this manner, the $1/\eta$ correction introduces a confining potential and lifts the vanishing energy gap at $g_c = 1$. In our case, such correction can become significant since N grows exponentially, and so does $\mathrm{Tr}[\rho(t)(a + a^\dagger)^4]$. Hence, we expect that the exponential scaling reported in Sec. IV holds as long as $f(g)\mathrm{Tr}[\mathcal{S}(s_m)\rho(0)\mathcal{S}^\dagger(s_m)(a + a^\dagger)^4] \ll \eta$, as otherwise the correction can no longer be considered as a perturbation and will significantly modify the Gaussian nature of the state and, consequently, the generated squeezing. The previous conditions allow us to define a maximum number of cycles, m^*, before the $1/\eta$ correction becomes relevant, i.e., $m^* \approx \ln_3 \eta$. Hence, for $\eta \approx 10^6$, we expect that the exponential scaling holds up to $m^* \approx 10$.

VI. CONCLUSIONS

In this article, we have reported a quantum metrological scheme that yields a quantum Fisher information that scales exponentially with the protocol duration time T. Such scheme is rooted in the nonadiabaticity of a cycle in the control parameter reaching a quantum critical point in fully connected models. In one cycle, the state acquires squeezing, which can be amplified under a suitable choice of parameters by subsequent cycles. As we show, after m cycles of a duration 2τ each, the quantum Fisher information scales as $I_\omega \propto 3^{T/\tau}$. This scaling is well captured by the recent bound put forward in Ref. [25], which in turn allows us to find approximated expressions for the quantum Fisher information. We discuss the potential deviations to this ideal scenario, such as finite-size effects or the effect of decoherence mechanisms. Supported by numerical simulations, we find that the exponential time-scaling precision is robust against decoherence effects, while the exponential advantage over the standard-quantum limited precision holds even for nonzero dissipation rates. In addition, as we argue, finite-size effects pose a limit to the maximum number of cycles that can be performed before the exponential

scaling breaks down. Based on our previous analysis [25], we also expect that this QFI bound can be saturated using standard homodyne or photon-counting measurements.

Our results, together with those reported recently by Gietka *et al.* [9], highlight that systems featuring a quantum phase transition are a valuable resource in quantum metrology as they can yield an exponential advantage for parameter estimation.

ACKNOWLEDGMENTS

L.G. acknowledges support from the Austrian Academy of Sciences (ÖAW) and by the Austrian Science Fund (FWF) through Grants No. P32299 (PHONED) and No. M3214 (ASYMM-LM). R.P. acknowledges support from the European Union's Horizon 2020 FET-Open project SuperQuLAN (Grant No. 899354). O.A. acknowledges support from the UK EPSRC EP/S02994X/1 and Newcastle University (Newcastle University Academic Track fellowship).

APPENDIX A: ROBUSTNESS OF THE SQUEEZING AGAINST FINITE-TIME CYCLES AND VARIATIONS IN g_τ

As commented in the main text, the state becomes squeezed after one cycle, whose squeezing parameter is given by $|s| = \ln(3)/2$ [cf. Eq. (7)]. Here we provide a brief derivation of this expression. For that, we follow [87]. The solution to the dynamics under Eq. (2) can be written in terms of the Ermakov-Milne equation, $\ddot{\xi}(t) + \omega^2(t)\xi(t) = 1/[4\xi^3(t)]$, where $\omega^2(t) = \omega^2[1 - g^2(t)]$ is the frequency of the harmonic oscillator at time t, and $\xi(t)$ is an effective width of the state, whose equilibrium value is $\xi(t) = [2\omega(t)]^{-1/2}$. In the $\omega\tau \to \infty$ limit, it is possible to find solutions to the above equation as a combination of Airy functions [87]. Indeed, for $\omega\tau \to \infty$, one can find the overlap between the ground and the evolved states upon a cycle $g(t)$, which is given by $f(2\tau) = \sin(\pi/3)$ (see Ref. [87] for more details). Since for $\langle x\rangle = \langle p\rangle = 0$ the Hamiltonian in Eq. (2) only produces squeezing in the state, and because $|\langle 0|\mathcal{S}(s)|0\rangle|^2 = \cosh^{-1}(|s|)$, it follows that $\cosh^{-1}(|s|) = \sin(\pi/3)$, which finally leads to $|s| = \ln(3)/2$.

This result holds to a good degree of approximation for $\omega\tau \gtrsim 1$ and $g_c - g_\tau \ll 1$. Let us denote $|s(\tau)|$ the squeezing parameter after one cycle $g(t)$ [cf. Eq. (6)] with duration 2τ (see Appendix C for details on how to obtain $|s|$ from $\mathbf{R}$). From numerical simulations, we find that $|s(\tau)| \approx |s|$ provided $g_c - g_\tau \ll 1$ and $\omega\tau \gtrsim 1$. Indeed, Fig. 4(a) shows the robustness of $|s(\tau)|$ when $g_\tau \neq g_c = 1$ but $|g_c - g_\tau| \ll 1$. On the one hand, if $g_\tau \ll g_c = 1$, the dynamics is not influenced by the critical point, so $|s| \approx 0$. In addition, for $g_\tau \lesssim g_c$, the larger τ, the more sensitive $|s(\tau)|$ becomes to deviations in g_τ. This is due to the finite-energy gap at $g < g_c$, that is, for $\tau \gg 1/\Delta(g_\tau)$ the evolution becomes adiabatic and Eq. (7) no longer holds. On the other hand, from numerical simulation, we find that finite-time corrections when $g_\tau = 1$ obey $|s| - |s(\tau)| \approx (27\omega\tau)^{-2/3}$ for $\omega\tau \gtrsim 1$ [cf. Fig. 4(b)]. Hence, by increasing $\omega\tau$, the resulting squeezing gets closer to the expected $|s| = \ln(3)/2$ at the price of losing robustness against potential deviations from $g_\tau = 1$. For $\omega\tau \to 0$, one trivially obtains $|s(\tau)| \approx 0$. For the numerical results presented in the main text, we consider $\omega\tau \sim O(10)$. In particular, for $\omega\tau = 8$,

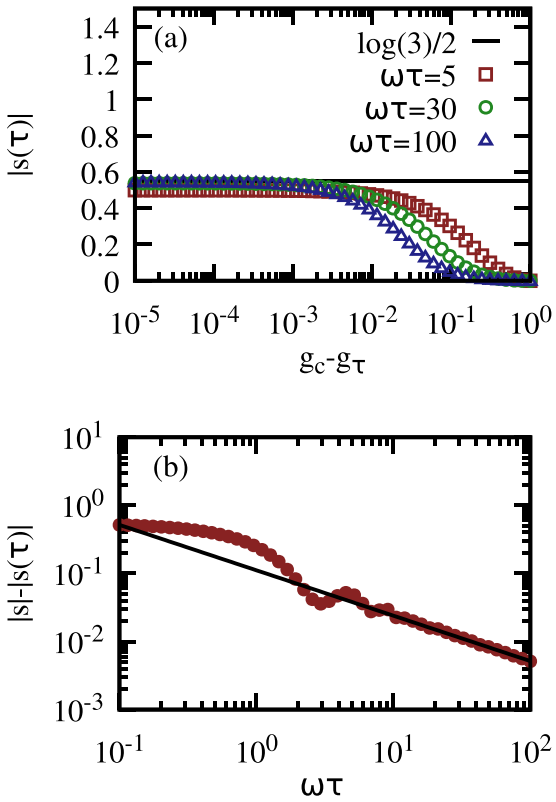

FIG. 4. Robustness of the squeezing parameter $|s(\tau)|$ achieved after one cycle under $g(t)$ in a total time 2τ, such that $g(0) = 0$ and $g(\tau) = g_\tau$, and for an initial vacuum state. (a) Squeezing $|s(\tau)|$ as a function of the deviation to the critical point $g_c - g_\tau$. The solid horizontal line corresponds to the expected $|s| = \ln(3)/2$, while the points have been obtained numerically for different $\omega\tau$ and g_τ values. (b) Finite-time corrections to the squeezing $|s(\tau)|$ when $g_\tau = 1$. The solid line corresponds to a best fit, $|s| - |s(\tau)| \approx (27\omega\tau)^{-2/3}$.

the difference between $|s(\tau)|$ and $|s|$ amounts to ≈0.03, and thus the expected exponential factor α, such that $Q_\omega \propto 3^{\alpha m}$, is $\alpha \approx 1.94$ [cf. Fig. 3(b)] rather than $\alpha = 2$ [cf. Eq. (11)], which would be reached in the limit $\omega\tau \to \infty$.

APPENDIX B: FINITE-TEMPERATURE INITIAL STATE

Let us consider an initial thermal state at inverse temperature $\beta = (k_B T)^{-1}$, $\rho_\beta = e^{-\beta H_0}/\mathrm{Tr}[e^{-\beta H_0}]$, where $H_0 = \omega a^\dagger a$ and $N_\beta = \mathrm{Tr}[\rho_\beta a^\dagger a] = (e^{\beta\omega} - 1)^{-1}$. As discussed in the main text, the state upon m cycles can acquire an m-fold squeezing $|s_m| = m|s|$, where $|s| = \ln(3)/2$, so that $\rho(2m\tau) = \mathcal{S}(s_m)\rho_\beta\mathcal{S}^\dagger(s_m)$, whose occupation number $N_m = \mathrm{Tr}[\rho(2m\tau)a^\dagger a]$ is given by

$$N_m = \tfrac{1}{2}[(2N_\beta + 1)\cosh(2|s_m|) - 1]. \tag{B1}$$

For $N_\beta = 0$, one recovers the expression in Eq. (9) when substituting $|s_m| = m\ln(3)/2$. From the bound (8) and again approximating $2N(t) + 1 \approx 2N_m + 1$ for $t \in [2(m-1)\tau, 2m\tau]$ and assuming $|s_m| \gtrsim 1$, we arrive at

$$I^B_\omega \approx 16\tau^2(2N_\beta + 1)^2\cosh^2(2|s_m|) \sim \tau^2 3^{T/\tau}, \tag{B2}$$

which is equivalent to Eq. (11) up to prefactors. The bound captures the exponential scaling. Yet, it becomes loose as it

overestimates I_ω since the N_β bosons originally contained in ρ_β do not actively participate in the parameter estimation.

APPENDIX C: SQUEEZING AND QUANTUM FISHER INFORMATION OF A GAUSSIAN STATE

A Gaussian state ρ is characterized by a Gaussian Wigner function in the phase space $\mathbf{X}^\top = (x, p)$, such that $W(\mathbf{X}) = P/(2\pi)\ e^{-(\mathbf{X}-\langle\mathbf{X}\rangle)^\top \mathbf{R}^{-1}(\mathbf{X}-\langle\mathbf{X}\rangle)}$, where $\langle\mathbf{X}^\top\rangle = (\langle x\rangle, \langle p\rangle)$ and $\mathbf{R}$ is the covariance matrix whose matrix elements are $R_{i,j} = \frac{1}{2}\langle X_i X_j + X_j X_i\rangle - \langle X_i\rangle\langle X_j\rangle$. In the previous equation for $W(\mathbf{X})$, $P = \det[\mathbf{R}]^{-1/2}$ denotes the purity of ρ [84]. Under the Hamiltonian $H(t) = \omega a^\dagger a - g^2(t)\omega(a + a^\dagger)^2/4$ and the master equation given in Eq. (14), it is straightforward to find the time-dependent Lyapunov equation for $\mathbf{R}$, which is given in Eq. (17). Recall that we employ $x = a + a^\dagger$ and $p = i(a^\dagger - a)$, so that $N = \mathrm{Tr}[\rho a^\dagger a] = (\mathrm{Tr}[\mathbf{R}] - 2)/4$, while we consider initial states with $\langle\mathbf{X}^\top\rangle = (0, 0)$ so that $\langle x\rangle = \langle p\rangle = 0\ \forall t$. For a decoherence-free evolution, the covariance matrix $\mathbf{R}$ fulfills $\det[\mathbf{R}] = 1$. Moreover, as the evolution produces only squeezing, it can be diagonalized at any time, $\tilde{\mathbf{R}} = \mathbf{V}\mathbf{R}\mathbf{V}^\top$ yielding $\mathrm{diag}[\tilde{\mathbf{R}}] = (e^{2|s|}, e^{-2|s|})$, while the angle θ follows from the eigenvectors of $\mathbf{R}$ in the phase space $\mathbf{X}$. That is, the eigenvector with eigenvalue $e^{-2|s|}$ is of the form $\mathbf{v}^\top = \mathbf{x}_s^\top = [\sin(\theta/2), \cos(\theta/2)]$.

In all the simulations presented in the main text, the derivatives $\partial_\omega\mathbf{R}$ and $\partial_\omega P$ have been computed numerically, setting $\epsilon/\omega \sim 10^{-8}$, which ensured the convergence of the results.

The phase θ upon one cycle can be estimated as follows. First, the phase gained during the evolution introduces a factor $e^{i\beta}$, where β reads

$$\beta = -\int_0^{2\tau} dt\ \sqrt{1 - g^2(t)} = -2\omega\tau \int_0^1 d\tilde{t}\sqrt{1 - g^2(\tilde{t})}, \tag{C1}$$

where $g(\tilde{t})$ is the protocol with a rescaled time $\tilde{t} = t/\tau$. That is, the state at time 2τ can be written as $|\psi(2\tau)\rangle = \sum_{n=0} c_n e^{i(n+1)\beta}|n\rangle$. In this manner, we can write $\beta = \omega\tau\nu$ with $\nu = -2\int_0^1 d\tilde{t}\ \sqrt{1 - g^2(\tilde{t})}$. Then, the phase θ changes linearly with $\omega\tau$, i.e.,

$$\theta = \nu\omega\tau + \theta_0, \tag{C2}$$

where $\theta_0 = \pi/2$ since, for $\omega\tau \to 0$, the evolution squeezes the state in the x direction. For a linear ramp, we find $\nu = -\pi/2$, so that $\theta = -\omega\tau\pi/2 + \pi/2$. For $\omega\tau = 2n$ with $n = 1, 2, \ldots$, one obtains $\theta = \pm\pi/2$. For subsequent cycles, the choice $\omega\tau = 2n$ leads to the desired phase-matching condition $\theta_{m+1} = \theta_m$.

[1] V. Giovannetti, S. Lloyd, and L. Maccone, Quantum-enhanced measurements: Beating the standard quantum limit, Science **306**, 1330 (2004).

[2] V. Giovannetti, S. Lloyd, and L. Maccone, Quantum Metrology, Phys. Rev. Lett. **96**, 010401 (2006).

[3] M. G. A. Paris, Quantum estimation for quantum technology, Intl. J. Quantum Inf. **07**, 125 (2009).

[4] L. Pezzè, A. Smerzi, M. K. Oberthaler, R. Schmied, and P. Treutlein, Quantum metrology with nonclassical states of atomic ensembles, Rev. Mod. Phys. **90**, 035005 (2018).

[5] J. P. Dowling and G. J. Milburn, Quantum technology: The second quantum revolution, Philos. Trans. R. Soc. London A **361**, 1655 (2003).

[6] S. L. Braunstein and C. M. Caves, Statistical Distance and the Geometry of Quantum States, Phys. Rev. Lett. **72**, 3439 (1994).

[7] S. Boixo, S. T. Flammia, C. M. Caves, and J. M. Geremia, Generalized Limits for Single-Parameter Quantum Estimation, Phys. Rev. Lett. **98**, 090401 (2007).

[8] S. M. Roy and S. L. Braunstein, Exponentially Enhanced Quantum Metrology, Phys. Rev. Lett. **100**, 220501 (2008).

[9] K. Gietka, L. Ruks, and T. Busch, Understanding and Improving Critical Metrology. Quenching Superradiant Light-Matter Systems Beyond the Critical Point, Quantum **6**, 700 (2022).

[10] S. Pang and A. N. Jordan, Optimal adaptive control for quantum metrology with time-dependent Hamiltonians, Nat. Commun. **8**, 14695 (2017).

[11] S. Sachdev, *Quantum Phase Transitions*, 2nd ed. (Cambridge University Press, Cambridge, 2011).

[12] P. Zanardi, M. G. A. Paris, and L. Campos Venuti, Quantum criticality as a resource for quantum estimation, Phys. Rev. A **78**, 042105 (2008).

[13] M. Bina, I. Amelio, and M. G. A. Paris, Dicke coupling by feasible local measurements at the superradiant quantum phase transition, Phys. Rev. E **93**, 052118 (2016).

[14] S. Fernández-Lorenzo and D. Porras, Quantum sensing close to a dissipative phase transition: Symmetry breaking and criticality as metrological resources, Phys. Rev. A **96**, 013817 (2017).

[15] M. M. Rams, P. Sierant, O. Dutta, P. Horodecki, and J. Zakrzewski, At the Limits of Criticality-Based Quantum Metrology: Apparent Super-Heisenberg Scaling Revisited, Phys. Rev. X **8**, 021022 (2018).

[16] L. Garbe, M. Bina, A. Keller, M. G. A. Paris, and S. Felicetti, Critical Quantum Metrology with a Finite-Component Quantum Phase Transition, Phys. Rev. Lett. **124**, 120504 (2020).

[17] P. A. Ivanov, Enhanced two-parameter phase-space-displacement estimation close to a dissipative phase transition, Phys. Rev. A **102**, 052611 (2020).

[18] Y. Chu, S. Zhang, B. Yu, and J. Cai, Dynamic Framework for Criticality-Enhanced Quantum Sensing, Phys. Rev. Lett. **126**, 010502 (2021).

[19] R. D. Candia, F. Minganti, K. V. Petrovnin, G. S. Paraoanu, and S. Felicetti, Critical parametric quantum sensing, arXiv:2107.04503.

[20] T. Ilias, D. Yang, S. F. Huelga, and M. B. Plenio, Criticality-enhanced quantum sensing via continuous measurement, PRX Quantum **3**, 010354 (2022).

[21] Y. Hu, J. Huang, J.-F. Huang, Q.-T. Xie, and J.-Q. Liao, Dynamic sensitivity of quantum Rabi model with quantum criticality, arXiv:2101.01504.

[22] A. Fallani, M. A. C. Rossi, D. Tamascelli, and M. G. Genoni, Learning feedback control strategies for quantum metrology, PRX Quantum **3**, 020310 (2022).

[23] D. Xie, C. Xu, and A. M. Wang, Quantum thermometry with a dissipative quantum Rabi system, arXiv:2105.12906.

[24] A. Niezgoda and J. Chwedeńczuk, Many-Body Nonlocality as a Resource for Quantum-Enhanced Metrology, Phys. Rev. Lett. **126**, 210506 (2021).

[25] L. Garbe, O. Abah, S. Felicetti, and R. Puebla, Critical quantum metrology with fully connected models: From Heisenberg to Kibble–Zurek scaling, Quantum Sci. Technol. **7**, 035010 (2022).

[26] V. Montenegro, U. Mishra, and A. Bayat, Global Sensing and Its Impact for Quantum Many-Body Probes with Criticality, Phys. Rev. Lett. **126**, 200501 (2021).

[27] P. A. Ivanov, Enhanced parameter estimation with periodically driven quantum probe, Entropy **23**, 1333 (2021).

[28] K. Gietka, Squeezing by critical speeding up: Applications in quantum metrology, Phys. Rev. A **105**, 042620 (2022).

[29] K. Gietka and T. Busch, Inverted harmonic oscillator dynamics of the nonequilibrium phase transition in the Dicke model, Phys. Rev. E **104**, 034132 (2021).

[30] T. Weiss, M. Roda-Llordes, E. Torrontegui, M. Aspelmeyer, and O. Romero-Isart, Large Quantum Delocalization of a Levitated Nanoparticle Using Optimal Control: Applications for Force Sensing and Entangling via Weak Forces, Phys. Rev. Lett. **127**, 023601 (2021).

[31] K. Yamamoto, S. Endo, H. Hakoshima, Y. Matsuzaki, and Y. Tokunaga, Error-mitigated quantum metrology, arXiv:2112.01850.

[32] F. Cosco, J. S. Pedernales, and M. B. Plenio, Enhanced force sensitivity and entanglement in periodically driven optomechanics, Phys. Rev. A **103**, L061501 (2021).

[33] R. Trényi, A. Lukács, P. Horodecki, R. Horodecki, T. Vértesi, and G. Tóth, Multicopy metrology with many-particle quantum states, arXiv:2203.05538.

[34] H. J. Lipkin, N. Meshkov, and A. Glick, Validity of many-body approximation methods for a solvable model, Nucl. Phys. **62**, 188 (1965).

[35] R. H. Dicke, Coherence in spontaneous radiation processes, Phys. Rev. **93**, 99 (1954).

[36] S. Ashhab, Superradiance transition in a system with a single qubit and a single oscillator, Phys. Rev. A **87**, 013826 (2013).

[37] L. Bakemeier, A. Alvermann, and H. Fehske, Quantum phase transition in the Dicke model with critical and noncritical entanglement, Phys. Rev. A **85**, 043821 (2012).

[38] M.-J. Hwang, R. Puebla, and M. B. Plenio, Quantum Phase Transition and Universal Dynamics in the Rabi Model, Phys. Rev. Lett. **115**, 180404 (2015).

[39] R. Puebla, M.-J. Hwang, and M. B. Plenio, Excited-state quantum phase transition in the Rabi model, Phys. Rev. A **94**, 023835 (2016).

[40] P. Ribeiro, J. Vidal, and R. Mosseri, Thermodynamical Limit of the Lipkin-Meshkov-Glick Model, Phys. Rev. Lett. **99**, 050402 (2007).

[41] P. Ribeiro, J. Vidal, and R. Mosseri, Exact spectrum of the Lipkin-Meshkov-Glick model in the thermodynamic limit and finite-size corrections, Phys. Rev. E **78**, 021106 (2008).

[42] C. Emary and T. Brandes, Quantum Chaos Triggered by Precursors of a Quantum Phase Transition: The Dicke Model, Phys. Rev. Lett. **90**, 044101 (2003).

[43] C. Emary and T. Brandes, Chaos and the quantum phase transition in the Dicke model, Phys. Rev. E **67**, 066203 (2003).

[44] N. Lambert, C. Emary, and T. Brandes, Entanglement and the Phase Transition in Single-Mode Superradiance, Phys. Rev. Lett. **92**, 073602 (2004).

[45] M. Liu, S. Chesi, Z.-J. Ying, X. Chen, H.-G. Luo, and H.-Q. Lin, Universal Scaling and Critical Exponents of the Anisotropic Quantum Rabi Model, Phys. Rev. Lett. **119**, 220601 (2017).

[46] L.-T. Shen, Z.-B. Yang, H.-Z. Wu, and S.-B. Zheng, Quantum phase transition and quench dynamics in the anisotropic Rabi model, Phys. Rev. A **95**, 013819 (2017).

[47] J. Peng, E. Rico, J. Zhong, E. Solano, and I. L. Egusquiza, Unified superradiant phase transitions, Phys. Rev. A **100**, 063820 (2019).

[48] H.-J. Zhu, K. Xu, G.-F. Zhang, and W.-M. Liu, Finite-Component Multicriticality at the Superradiant Quantum Phase Transition, Phys. Rev. Lett. **125**, 050402 (2020).

[49] S. Felicetti and A. Le Boité, Universal Spectral Features of Ultrastrongly Coupled Systems, Phys. Rev. Lett. **124**, 040404 (2020).

[50] L.-T. Shen, J.-W. Yang, Z.-R. Zhong, Z.-B. Yang, and S.-B. Zheng, Quantum phase transition and quench dynamics in the two-mode Rabi model, Phys. Rev. A **104**, 063703 (2021).

[51] F. Minganti, L. Garbe, A. Le Boité, and S. Felicetti, Non-Gaussian superradiant transition via three-body ultrastrong coupling, arXiv:2204.03520.

[52] S. Dusuel and J. Vidal, Finite-Size Scaling Exponents of the Lipkin-Meshkov-Glick Model, Phys. Rev. Lett. **93**, 237204 (2004).

[53] J. Vidal and S. Dusuel, Finite-size scaling exponents in the Dicke model, Europhys. Lett. **74**, 817 (2006).

[54] V. M. Bastidas, C. Emary, B. Regler, and T. Brandes, Nonequilibrium Quantum Phase Transitions in the Dicke Model, Phys. Rev. Lett. **108**, 043003 (2012).

[55] R. Puebla, A. Relaño, and J. Retamosa, Excited-state phase transition leading to symmetry-breaking steady states in the Dicke model, Phys. Rev. A **87**, 023819 (2013).

[56] T. Brandes, Excited-state quantum phase transitions in dicke superradiance models, Phys. Rev. E **88**, 032133 (2013).

[57] R. Puebla and A. Relaño, Irreversible processes without energy dissipation in an isolated Lipkin-Meshkov-Glick model, Phys. Rev. E **92**, 012101 (2015).

[58] R. Puebla, M.-J. Hwang, J. Casanova, and M. B. Plenio, Probing the Dynamics of a Superradiant Quantum Phase Transition with a Single Trapped Ion, Phys. Rev. Lett. **118**, 073001 (2017).

[59] L. Garbe, I. L. Egusquiza, E. Solano, C. Ciuti, T. Coudreau, P. Milman, and S. Felicetti, Superradiant phase transition in the ultrastrong-coupling regime of the two-photon Dicke model, Phys. Rev. A **95**, 053854 (2017).

[60] Y. Wang, W.-L. You, M. Liu, Y.-L. Dong, H.-G. Luo, G. Romero, and J. Q. You, Quantum criticality and state engineering in the simulated anisotropic quantum rabi model, New J. Phys. **20**, 053061 (2018).

[61] B. Žunkovič, M. Heyl, M. Knap, and A. Silva, Dynamical Quantum Phase Transitions in Spin Chains with Long-Range Interactions: Merging Different Concepts of Nonequilibrium Criticality, Phys. Rev. Lett. **120**, 130601 (2018).

[62] M.-J. Hwang, P. Rabl, and M. B. Plenio, Dissipative phase transition in the open quantum Rabi model, Phys. Rev. A **97**, 013825 (2018).

[63] M.-J. Hwang, B.-B. Wei, S. F. Huelga, and M. B. Plenio, Universality in the decay and revival of Loschmidt echoes, arXiv:1904.09937.

[64] R. Puebla, A. Smirne, S. F. Huelga, and M. B. Plenio, Universal Anti-Kibble-Zurek Scaling in Fully Connected Systems, Phys. Rev. Lett. **124**, 230602 (2020).

[65] R. Puebla, Finite-component dynamical quantum phase transitions, Phys. Rev. B **102**, 220302(R) (2020).

[66] A. L. Corps and A. Relaño, Constant of Motion Identifying Excited-State Quantum Phases, Phys. Rev. Lett. **127**, 130602 (2021).

[67] T. Zibold, E. Nicklas, C. Gross, and M. K. Oberthaler, Classical Bifurcation at the Transition from Rabi to Josephson Dynamics, Phys. Rev. Lett. **105**, 204101 (2010).

[68] K. Baumann, C. Guerlin, F. Brennecke, and T. Esslinger, Dicke quantum phase transition with a superfluid gas in an optical cavity, Nature (London) **464**, 1301 (2010).

[69] K. Baumann, R. Mottl, F. Brennecke, and T. Esslinger, Exploring Symmetry Breaking at the Dicke Quantum Phase Transition, Phys. Rev. Lett. **107**, 140402 (2011).

[70] R. Mottl, F. Brennecke, K. Baumann, R. Landig, T. Donner, and T. Esslinger, Roton-type mode softening in a quantum gas with cavity-mediated long-range interactions, Science **336**, 1570 (2012).

[71] P. Jurcevic, H. Shen, P. Hauke, C. Maier, T. Brydges, C. Hempel, B. P. Lanyon, M. Heyl, R. Blatt, and C. F. Roos, Direct Observation of Dynamical Quantum Phase Transitions in an Interacting Many-Body System, Phys. Rev. Lett. **119**, 080501 (2017).

[72] M.-L. Cai, Z.-D. Liu, W.-D. Zhao, Y.-K. Wu, Q.-X. Mei, Y. Jiang, L. He, X. Zhang, Z.-C. Zhou, and L.-M. Duan, Observation of a quantum phase transition in the quantum Rabi model with a single trapped ion, Nat. Commun. **12**, 1126 (2021).

[73] Z. Zhiqiang, C. H. Lee, R. Kumar, K. Arnold, S. J. Masson, A. Parkins, and M. Barrett, Nonequilibrium phase transition in a spin-1 Dicke model, Optica **4**, 424 (2017).

[74] A. Dareau, Y. Meng, P. Schneeweiss, and A. Rauschenbeutel, Observation of Ultrastrong Spin-Motion Coupling for Cold Atoms in Optical Microtraps, Phys. Rev. Lett. **121**, 253603 (2018).

[75] D. Lv, S. An, Z. Liu, J.-N. Zhang, J. S. Pedernales, L. Lamata, E. Solano, and K. Kim, Quantum Simulation of the Quantum Rabi Model in a Trapped Ion, Phys. Rev. X **8**, 021027 (2018).

[76] A. Safavi-Naini, R. J. Lewis-Swan, J. G. Bohnet, M. Gärttner, K. A. Gilmore, J. E. Jordan, J. Cohn, J. K. Freericks, A. M. Rey, and J. J. Bollinger, Verification of a Many-Ion Simulator of the Dicke Model Through Slow Quenches across a Phase Transition, Phys. Rev. Lett. **121**, 040503 (2018).

[77] Q.-X. Mei, B.-W. Li, Y.-K. Wu, M.-L. Cai, Y. Wang, L. Yao, Z.-C. Zhou, and L.-M. Duan, Experimental Realization of the Rabi-Hubbard Model with Trapped Ions, Phys. Rev. Lett. **128**, 160504 (2022).

[78] D. Marković, S. Jezouin, Q. Ficheux, S. Fedortchenko, S. Felicetti, T. Coudreau, P. Milman, Z. Leghtas, and B. Huard, Demonstration of an Effective Ultrastrong Coupling between Two Oscillators, Phys. Rev. Lett. **121**, 040505 (2018).

[79] D. Bothner, I. Rodrigues, and G. Steele, Photon-pressure strong coupling between two superconducting circuits, Nat. Phys. **17**, 85 (2021).

[80] R.-H. Zheng, W. Ning, Y.-H. Chen, J.-H. Lü, L.-T. Shen, K. Xu, Y.-R. Zhang, D. Xu, H. Li, Y. Xia, F. Wu, Z.-B. Yang, A. Miranowicz, N. Lambert, D. Zheng, H. Fan, F. Nori, and S.-B. Zheng, Emergent Schrödinger cat states during superradiant phase transitions, arXiv:2207.05512.

[81] G. A. Peterson, S. Kotler, F. Lecocq, K. Cicak, X. Y. Jin, R. W. Simmonds, J. Aumentado, and J. D. Teufel, Ultrastrong Parametric Coupling between a Superconducting Cavity and a Mechanical Resonator, Phys. Rev. Lett. **123**, 247701 (2019).

[82] J. Rieser, M. A. Ciampini, H. Rudolph, N. Kiesel, K. Hornberger, B. A. Stickler, M. Aspelmeyer, and U. Delić, Tunable light-induced dipole-dipole interaction between optically levitated nanoparticles, Science **377**, 987 (2022).

[83] X. Chen, Z. Wu, M. Jiang, X.-Y. Lü, X. Peng, and J. Du, Experimental quantum simulation of superradiant phase transition beyond no-go theorem via antisqueezing, Nat. Commun. **12**, 6281 (2021).

[84] O. Pinel, P. Jian, N. Treps, C. Fabre, and D. Braun, Quantum parameter estimation using general single-mode Gaussian states, Phys. Rev. A **88**, 040102(R) (2013).

[85] A. Ferraro, S. Olivares, and M. Paris, *Gaussian States in Quantum Information* (Bibliopolis, Napoli, 2005).

[86] A. Polkovnikov and V. Gritsev, Breakdown of the adiabatic limit in low-dimensional gapless systems, Nat. Phys. **4**, 477 (2008).

[87] N. Defenu, Quantum adiabatic cycles and their breakdown: An analytic solution, Commun. Phys. **4**, 150 (2021).

[88] O. Abah, G. De Chiara, M. Paternostro, and R. Puebla, Harnessing nonadiabatic excitations promoted by a quantum critical point: Quantum battery and spin squeezing, Phys. Rev. Res. **4**, L022017 (2022).

[89] M. Rashid, T. Tufarelli, J. Bateman, J. Vovrosh, D. Hempston, M. S. Kim, and H. Ulbricht, Experimental Realization of a Thermal Squeezed State of Levitated Optomechanics, Phys. Rev. Lett. **117**, 273601 (2016).

[90] H.-P. Breuer and F. Petruccione, *The Theory of Open Quantum Systems* (Oxford University Press, Oxford, 2002).